Chemical Geology 436 (2016) 11–23

Contents lists available at ScienceDirect

Chemical Geology

journal homepage: www.elsevier.com/locate/chemgeo

Chemical and isotopic signatures of waters associated with the carbonation of ultramafic mine tailings, Woodsreef Asbestos Mine, Australia

H.C. Oskierski [a,*], B.Z. Dlugogorski [a], T.K. Oliver [b], G. Jacobsen [c]

[a] School of Engineering and Information Technology, Murdoch University, Murdoch, WA 6150, Australia
[b] School of Engineering, The University of Newcastle, Callaghan, NSW, 2308, Australia
[c] Australian Nuclear Science and Technology Organisation (ANSTO), Institute for Environmental Research, Locked Bag 2001, Kirrawee DC, NSW 2234, Australia

ARTICLE INFO

Article history:
Received 3 February 2016
Received in revised form 10 April 2016
Accepted 17 April 2016
Available online 28 April 2016

Keywords:
Serpentinite
Hydromagnesite
Mine tailings
Mineral carbonation
CO_2 sequestration
Carbonation mechanisms
Degassing of CO_2
Evaporation
Isotope fractionation

ABSTRACT

Extensive carbonate crusts have formed on the tailings of the Woodsreef Asbestos Mine, sequestering significant amounts of CO_2 directly from the atmosphere. The physico-chemical (pH, *T*, conductivity), chemical (cations, dissolved inorganic carbon (DIC)) and isotopic (δ^2H, $\delta^{18}O$, $\delta^{13}C_{DIC}$, $F^{14}C$) signatures of waters interacting with the tailings and associated carbonate precipitates provide insight into the processes controlling carbonation. We observe two distinct evolutionary pathways for a set of stream and meteoric-derived water samples, respectively, with both groups generally being characterised as moderately alkaline, bicarbonate-dominated and Mg-rich waters. Stream water samples are supersaturated with CO_2 and therefore prone to degassing, which, in combination with evaporation, drives carbonate supersaturation and precipitation. Isotopic signatures indicate soil CO_2 as the main carbon source in the stream waters entering the tailings pile, whereas water emerging downstream of the tailings pile may also contain carbon from the dissolution of isotopically light bedrock magnesite in an open system with respect to soil CO_2. The evolution of meteoric-derived waters on the other hand, partly occurs under CO_2-limited conditions, which results from reduced CO_2 ingress at depth and/or a temporal lag between fluid alkalisation and kinetically hindered uptake of CO_2 into alkaline solution. A high pH, Mg-rich meteoric water absorbs atmospheric CO_2 after discharging into a tunnel within the tailings pile, resulting in high DIC concentrations with atmospheric carbon isotope signature. Evaporation of the water at the discharge point in the tunnel drives precipitation of hydromagnesite ($Mg_5(CO_3)_4(OH)_2 \cdot 4H_2O$), displaying a clear atmospheric isotope signature, broadly consistent with previous estimates of carbon and oxygen isotope fractionation during precipitation of hydrated Mg-carbonate.

1. Introduction

An earlier study has shown that, weathering of the mine tailings at the Woodsreef Asbestos Mine, NSW, Australia results in the formation of extensive carbonate crusts and cements (Oskierski et al., 2013a). The crusts, consisting mainly of hydromagnesite, predominantly incorporate CO_2 of atmospheric origin, as evidenced by high $\delta^{13}C$ and $F^{14}C$. Weathering-related carbonation of silicate rocks is considered an important process for the stabilisation of Earth's climate and contributes significantly to the removal of CO_2 from the atmosphere (Gaillardet et al., 1999; Ruddiman, 2013). Quantification of carbonate content in ultramafic tailings based on quantitative X-ray diffraction demonstrates that carbonation proceeds at significantly higher rates than background CO_2 uptake rates by chemical weathering of coherent silicate rock (Oskierski et al., 2013a; Wilson et al., 2009; Wilson et al., 2011; Wilson et al., 2014). Consequently carbonation of ultramafic mine tailings provides a viable option for low-energy, low-cost sequestration of atmospheric CO_2, which has the potential to make a relevant contribution to international efforts in reducing CO_2 concentrations in the atmosphere (Assima et al., 2014a; Assima et al., 2014b; Power et al., 2013; Power et al., 2014; Pronost et al., 2011; Wilson et al., 2006; Wilson et al., 2014).

Since dissolution of tailings minerals and precipitation of carbonate occur in the aqueous phase, water samples provide valuable insight into the processes controlling carbonation. Water samples represent an intermediate step in the aqueous carbonation process and thus add detail to the understanding of natural carbonation of mine tailings during weathering, which has so far been largely based on mineralogy and isotopic signatures of solid samples (Oskierski et al., 2013a; Pronost et al., 2012; Wilson et al., 2006; Wilson et al., 2009), except for a study of biogeochemical processes in hydromagnesite playas (Power et al., 2009) and of water infiltrating peridotite-hosted mine shafts (Beinlich and Austrheim, 2012). Reactive transport models have been used to

* Corresponding author.
E-mail address: H.Oskierski@murdoch.edu.au (H.C. Oskierski).

http://dx.doi.org/10.1016/j.chemgeo.2016.04.014
0009-2541/

derive a better understanding of the formation of alkaline, Ca–OH waters emanating from ultramafic rocks (Bruni et al., 2002; Cipolli et al., 2004; Marques et al., 2008; Paukert et al., 2012) and more recently these models are also applied to the carbonation of ultramafic mine tailings (Bea et al., 2011; Harrison et al., 2015; Wilson et al., 2014).

In this contribution, we integrate sampling context, field parameters, water chemistry and isotopic information on carbon sources and evaporation to derive insight into the evolution of water samples associated with the carbonation of mine tailings at Woodsreef, with special emphasis on carbonate precipitation. Enhanced understanding of carbonation of mine tailings aims to identify rate-limiting steps in the carbonation process in order to engineer tailings storage facilities optimised for the purpose of CO_2 sequestration (Assima et al., 2012; Assima et al., 2013a; Assima et al., 2014a; Assima et al., 2014b; Gras et al., 2015; Gras et al., 2015; Lechat et al., 2015; Lechat et al., 2016; McCutcheon et al., 2015; Power et al., 2013; Power et al., 2014; Pronost et al., 2011; Pronost et al., 2012; Wilson et al., 2014).

2. Study site

2.1. Geology

The Woodsreef Asbestos Deposit, New South Wales, Australia, is located in the southern part of the New England Orogen, which stretches along the central area of the east coast of the Australian continent (Fig. 1). The deposit is a chrysotile mineralisation hosted in the ultramafic rocks of the Great Serpentinite Belt, a disrupted ophiolite sequence which has been tectonically emplaced along the Peel–Manning Fault system. The Woodsreef serpentinite predominantly consists of schistose and massive serpentinite, as well as partially serpentinised harzburgite (Glen and Butt, 1981). Chrysotile was extracted from the deposit intermittently between 1906 and 1983, producing 24.2 Mt of ultramafic tailings (Brown et al., 1992). The tailings result from dry-grinding of chrysotile ore and are stored above ground on an area covering about 0.5 km^2 (Svanosio, 2000; Fig. 1).

On the western side the Woodsreef serpentinite, a thin layer of magnesite and chlorite creates a sharp boundary to the sandstones of the Tamworth Belt, while the eastern boundary to the rocks of the Woolomin group is much more irregular (Glen and Butt, 1981). Siliceous argillites, chert and jasper, with minor diamictites and metabasalt of the pelagic Nangarah and Bobs Creek Formations constitute the lithologies of the Woolomin Group to the east of the Woodsreef serpentinite (Vickery et al., 2010). For a detailed description of the geology of the study area and the chrysotile mineralisation the reader is referred to Glen and Butt (1981); O'Hanley and Offler (1992) and Vickery et al. (2010).

2.2. Mineralogy

The mineralogy of the tailings pile at Woodsreef is a result of several stages of alteration, including serpentinisation–recrystallisation, hydrothermal alteration and weathering of the bedrock (Ashley and Brownlow, 1993; Ashley, 1997; Kmetoni, 1984; O'Hanley and Offler,

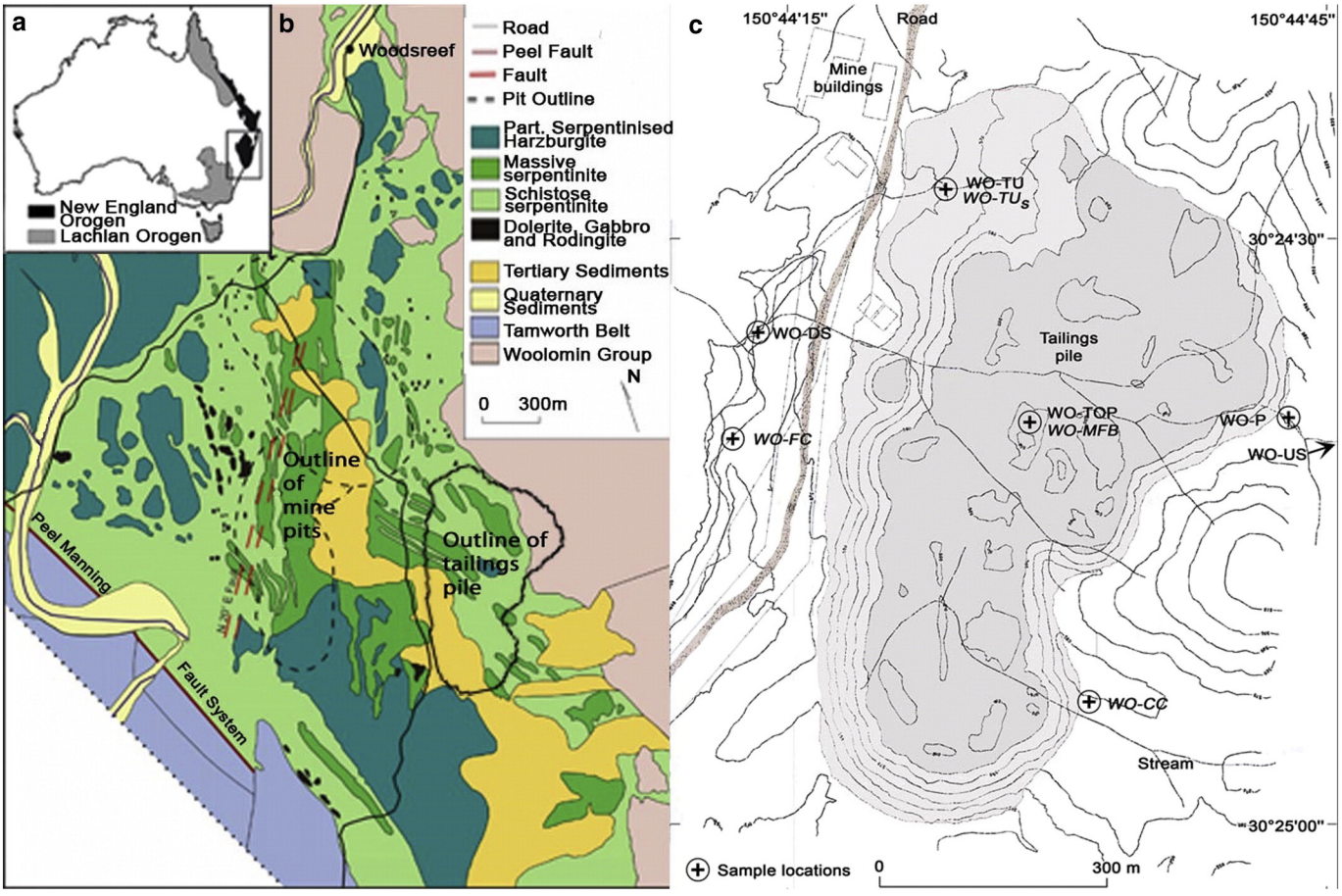

Fig. 1. Geology and sample locations (modified from Oskierski et al., 2013a). a. Location of the Southern New England Orogen (modified from Guo et al., 2007). b. Detailed geology of the Woodsreef serpentinite (modified from Davis, 2008 and Glen, 1971). c. Topography of tailings pile and sampling locations (modified from Svanosio, 2000).

Table 1
Summary of minerals observed in earlier studies of the Woodsreef serpentinite and tailings.

	Alteration type	Associated minerals and relative abundance in the tailings pile[a]
Alteration of bedrock	Harzburgite protolith	Forsterite*, diopside*, enstatite*
	Serpentinisation–recrystallisation (1)[b]	(Tremolite), (chlorite), (talc), (antigorite), magnetite*
	Serpentinisation–recrystallisation (2)[b]	Lizardite****, brucite*, magnetite*
	Serpentinisation–recrystallisation (3)[b]	Lizardite****, chrysotile*, magnetite*
	Weathering-carbonation	(Clay minerals)[c], hematite*, magnesite*, calcite*, dolomite*, opal A*, quartz*, pyroaurite**[d]
Alteration of tailings	Weathering-carbonation	Hydromagnesite**, pyroaurite**[d]
Not assigned to specific alteration[e]		(Coalingite), (huntite), (grossularit), (sepiolite), (palygorskite), (ilmenite), (mica), (spinel), (amphibol), (anthophyllite), (pyrite), (chromite)

****Predominant; ***subdominant; **abundant; *minor; *trace; (mineral) not observed in Oskierski et al. (2013a).
[a] Relative abundances from Oskierski et al. (2013a).
[b] From O'Hanley and Offler (1992).
[c] Saponite, montmorillionite (Caillaud et al., 2006).
[d] Pyroaurite may have partially formed during weathering of the bedrock before extraction.
[e] From Kmetoni (1984).

1992; O'Hanley, 1996) as well as in-situ weathering of the tailings pile after mining (Oskierski et al., 2013a). Table 1 summarises the results of earlier mineralogical studies.

2.3. Climate and sample locations

The climate at Woodsreef is semi-arid, with mean rainfall between 39.3 and 87.5 mm per month and average temperatures ranging between 0.3 and 31.8 °C (Australian Government Bureau of Meteorology). Due to the relatively low amount of rainfall (average of 3.8 to 7 days per month with more than 1 mm rainfall, Australian Government Bureau of Meteorology) and the ephemeral nature of most of the sampled waters, a continuous sampling programme could not be established. Water samples were taken from 5 different locations throughout the tailings pile (Fig. 1) and from a rainwater tank at Manilla, about 60 km south of Woodsreef (Table 2).

A stream flowing through country rocks of the Woolomin Group was sampled upriver of the tailings pile (WO-US, Woodsreef upstream) and at the point where the tailings intercept the stream and a pond forms at the eastern base of the tailings pile (WO-P, Woodsreef pond, Fig. 2b). Another water (WO-DS, Woodsreef downstream) that is potentially genetically related (i.e. that has formed through evolution of the other water samples) was sampled on the western side of the tailings where an ephemeral stream re-emerges to the surface after interaction with tailings material and the possible addition from other contributing streams (see streams in Fig. 1c). The sample from a water tank in Manilla (MWT, Manilla water tank) is taken to represent meteoric water in the study area (Oskierski et al., 2013b). Samples were taken from a depression on top of the tailings pile (WO-TOP, Fig. 2d) and from drip water emerging within a tunnel in the tailings material (WO-TU, Fig. 2e), either on the same day or the day after a rainfall. Due to the slow drip rate the latter sample has partly equilibrated with atmospheric CO_2 during sampling. The tunnel is circular with a diameter of about 3 m and penetrates about 10 m downwards into the tailings. At the deepest point of the tunnel a steel grid in the ceiling is covered by 20 to 30 cm wide serpentinite chunks, through which water percolates into the tunnel.

Solid samples were taken to be as closely related to the water samples as possible, i.e., precipitate from the discharge point of the drip water (WO-TU_s, $tunnel_{solid}$) and the sediments from the depression on top of the tailings (WO-MFB) and downstream of water sample WO-DS (WO-FC, Woodsreef flow channel). A cobble-coating has also been sampled at the south-eastern base of the tailings pile (WO-CC, Fig. 2f).

3. Sampling and analytical methods

3.1. Field parameters and sampling of waters

We measured pH, temperature and conductivity of fresh water samples directly in the field using a pH/conductivity meter and a thermocouple. The pH meter was calibrated using pH standards (pH 4.0, 7.0, 11.0) each day prior to use in the field and stability of the calibration was confirmed throughout the day using the pH 7.0 standard.

3.2. Cations

One aliquot of 250 to 500 mL was acidified to pH <2 in the field using concentrated nitric acid for determination of cation concentrations using a Varian 715-ES ICP-OES. Sample aliquots were stored cold until analysis and measured both undiluted and diluted volumetrically as required for more concentrated cations such as Mg. Merck ICP multi-element standard solutions were used for calibration and quality control along with per analysis grade nitric acid, resulting in detection limits in the ppb range. Repeat analysis of water samples indicates relative reproducibility of about 10% (2σ).

3.3. Carbon and oxygen isotopes and DIC

The $\delta^{13}C$ of dissolved inorganic carbon (DIC) in water samples was analysed using a GV2003 continuous flow isotope ratio mass spectrometer and headspace equilibration following a method modified from Assayag et al. (2006). Analysis was carried out as soon as possible, i.e., no later than 2–3 days after sampling. A volume of 1 mL of water sample and 0.2 mL of phosphoric acid were injected into a He-flushed septum vial, which was left to equilibrate for at least 24 h. $\delta^{13}C_{DIC}$ was calibrated via aqueous in-house and international reference standards and reported relative to VPDB. All analyses were carried out in triplicate and results represent averages. Reproducibility was better than 0.1 ‰ (1σ). Injection of water samples, directly into pre-acidified, He-flushed vials in the field, yielded identical $\delta^{13}C_{DIC}$ values confirming the veracity of the protocol for sample preparation. DIC concentrations were determined from the $m/z = 44$ signal intensity of the first CO_2 pulse as in previously established methods (Assayag et al., 2006; Salata et al., 2000). DIC concentration was calibrated using a range of gravimetric in-house standards. The $\delta^{13}C_{DIC}$ of sample MWT was determined once at the Environmental Analysis Laboratory, Southern Cross University. The $\delta^{13}C$ and $\delta^{18}O$ of carbonate samples were determined by CF-IRMS using standard methods as described in earlier work (Oskierski et al., 2013c). In brief, samples were loaded into septum vials, He-flushed and dissolved in 0.05 to 0.1 mL of 103% phosphoric acid at 72 °C for at least 16 h. We corrected the value of $\delta^{18}O$ for reaction with phosphoric acid using the fractionation factor of Das Sharma et al. (2002). Repeated analysis of an internal working standards was used to determine the external precision (1σ) as <0.05‰ for $\delta^{13}C$ and <0.1‰ for $\delta^{18}O$. The radiocarbon content of DIC in water and of carbonate samples was measured by Accelerator Mass Spectrometry (AMS) at the Australian Nuclear Science and Technology Organisation (ANSTO) following standard procedures (Fink et al., 2004). Results are reported as % modern carbon (pMC) but displayed in diagrams as fraction of modern carbon, with $F^{14}C = 1$ approximately equivalent to 100% modern carbon.

Table 2
Cation concentrations, field parameters, isotopic composition and carbonate system parameters in waters.

Sample	WO-TU	WO-TOP	MWT	WO-US	WO-P	WO-DS
Context	Drip water discharging into tunnel	Water in depression on tailings	Rainwater from water tank	Stream, upriver from tailings	Water pond base of tailings	Emerging downstream of tailings
Coordinates	−30.407788	−30.411253	−30.744331	−30.411400	−30.411468	−30.409505
	150.739534	150.740536	150.728454	150.746061	150.744819	150.737331
Mg (mg/L)	133.0	18.5	0.2	48[a]	34.0	158.0
Ca (mg/L)	1.8	1.6	0.5	85[a]	38.0	7.0
Si (mg/L)	1.1	0.2[b]	0.1	17.1	10.8	23.6
Na (mg/L)	1.9	1.9	0.1	29[a]	18.1	11.4
K (mg/L)	0.8	0.7	0.3	1.9	2.9	1.0
Fe (mg/L	<d.l.	<d.l.	0.2	<d.l.	<d.l.	<d.l.
Al (mg/L)	<d.l.	<d.l.	0.1	<d.l.	<d.l.	<d.l.
$\delta^{13}C_{graphite}$ (‰, VPDB) (1σ)	−5.0 (0.1)	n.d.	−8.0 (0.4)[c]	n.d.	n.d.	n.d.
pMC (%) (1σ)[*]	106.44 (0.29)	n.d.	105.90 (0.53)[c]	n.d.	n.d.	n.d.
Convent. radiocarbon age (yBP)	Modern	n.d.	Modern[c]	n.d.	n.d.	n.d.
$\delta^{13}C_{DIC}$ (‰, VPDB) (1σ)	−2.7 (0.1)[d]	−4.0 (0.1)[d]	−2.9 (0.1)[e]	−12.2 (0.1)[d]	−9.6 (0.1)[d]	−15.9 (0.1)[d]
$\delta^{2}H_{water}$ (‰, VSMOW) (1σ)	−24.7 (0.1)	−23.9 (0.1)	−20.5 (0.1)	−22.9 (0.1)	−15.6 (0.2)	−23.9 (0.1)
$\delta^{2}H_{water}$ (repeat)		−24.4 (0.1)	−20.4 (0.2)	−23.1 (0.1)		
$\delta^{18}O_{water}$ (‰, VSMOW) (1σ)	−4.2 (0.02)	−3.1 (0.06)	−4.0 (0.04)	−4.1 (0.03)	−2.6 (0.04)	−4.3 (0.05)
$\delta^{18}O_{water}$ (repeat)		−3.3 (0.05)	−4.1 (0.11)	−4.0 (0.06)		
T (°C)	17.2	28.8	24.5	21.6	29.3	21.1
Conductivity (μS/cm)	860	150	n.d.	750	510	1000
pH	9.1	8.4	6.1	7.8	8.3	7.5
DIC (mmol/L)	8.7	1.1	0.01[f]	6.4	4.0	9.1
pCO_2 (μatm)[**]	300	280		5400	1200	22,400
DIC eq CO_2 (mmol/L)[***]	8.9	1.1		5.6	3.7	7.2
pH eq CO_2[†]	9.0	8.3		8.9	8.7	8.9
Ratio pCO_2[‡]	0.77	0.72		13.8	3.1	57.4
Ratio DIC[#]	0.98	0.99		1.14	1.06	1.26

<d.l. — below detection limit.
n.d. — not determined.
[a] Concentration above calibrated range.
[b] Concentration below calibrated range.
[c] From Oskierski et al., 2013b.
[d] Average of triplicate measurements shown.
[e] Measured at Environmental Analysis Laboratory, Southern Cross University.
[f] DIC calculated for equilibrium with atmospheric CO_2.
[*] pMC = percent modern carbon.
[**] Theoretical pCO_2 of atmosphere in equilibrium with water sample, rounded to ±10 μatm.
[***] Theoretical DIC concentration of DIC in equilibrium with atmospheric CO_2 at pCO_2 of 350 μatm.
[†] Theoretical pH after equilibration with atmospheric CO_2 at pCO_2 of 350 μatm.
[‡] Ratio $pCO_{2sample}/pCO_{2atmosphere}$.
[#] Ratio of measured DIC and DIC eq CO_2.

3.4. Hydrogen and oxygen isotope signatures of waters

Another aliquot of water was sampled for analysis of δ^2H and $\delta^{18}O$ carried out at ANSTO. A H-device and Gasbench II connected to a Delta V Advantage Isotope Ratio Mass Spectrometer were deployed, respectively, for δ^2H and $\delta^{18}O$. Alternatively, a Picarro L2120-I Water Analyser served for the same analyses. IRMS and CRDS techniques were cross-verified via ANSTO in-house standards (AILS), which were calibrated against VSMOW2 and SLAP2. Results are reported relative to VSMOW2. Precision, given as 1σ relative error in Table 2, is better than 0.2‰ and 0.11‰ for δ^2H and $\delta^{18}O$, respectively.

3.5. Phase identification

Mineral phases in solid samples were identified in patterns collected on a Phillips X'Pert MPD X-ray diffractometer using Cu Kα, a scanning step size of 0.02° 2θ and a scan step time of 1 s over a range of 5 to 90° 2θ and matched against International Centre for Diffraction Data (ICDD).

3.6. Geochemical modelling

Geochemical modelling of saturation indices, pCO_2 of solutions, equilibration with atmospheric CO_2 (degassing/CO_2 uptake), evaporation and dissolution/precipitation of relevant minerals was carried out in PHREEQC (Parkhurst and Appelo, 1999). Since all of the analysed solutions are freshwaters with total dissolved solids of less than 500 mg/L, we used the wateq4f database available in PHREEQC. All sampled waters are bicarbonate dominated. A previous study of water quality has found <59 ppm, <22 ppm and <19 ppm of chloride, sulfate and nitrate ions, respectively, in relevant waters from the Woodsreef area (Toyer and Main, 1978). We did not determine concentrations of these anions and consequently errors on the charge balance ((cations − anions) / (cations + anions) × 100) range between 10 and 25%. Tables SI 1 and SI 2 in the online version at http://dx.doi.org/10.1016/j.chemgeo.2016.04.014. in the supplementary information provide a summary of thermodynamic modelling in PHREEQC, illustrating possible pathways for the evolution of chemical parameters and saturation indices in stream and meteoric waters, respectively.

To discuss the tendency of waters to degas or absorb CO_2, we calculate the partial pressure of CO_2 (pCO_2 in μatm) of a hypothetical atmosphere in equilibrium with the water sample. In this analysis, implicit in the PHREEQC model, the DIC can be represented by the aqueous carbon species included in Eqs. (1) and (2):

$$[DIC] = [CO_2^*] + [HCO_3^-] + \left[CO_3^{2-} + CaCO_3\right] + \left[CaHCO_3^+\right] + [MgCO_3] + \left[MgHCO_3^+\right] + [NaHCO_3] + \left[NaCO_3^-\right] \quad (1)$$

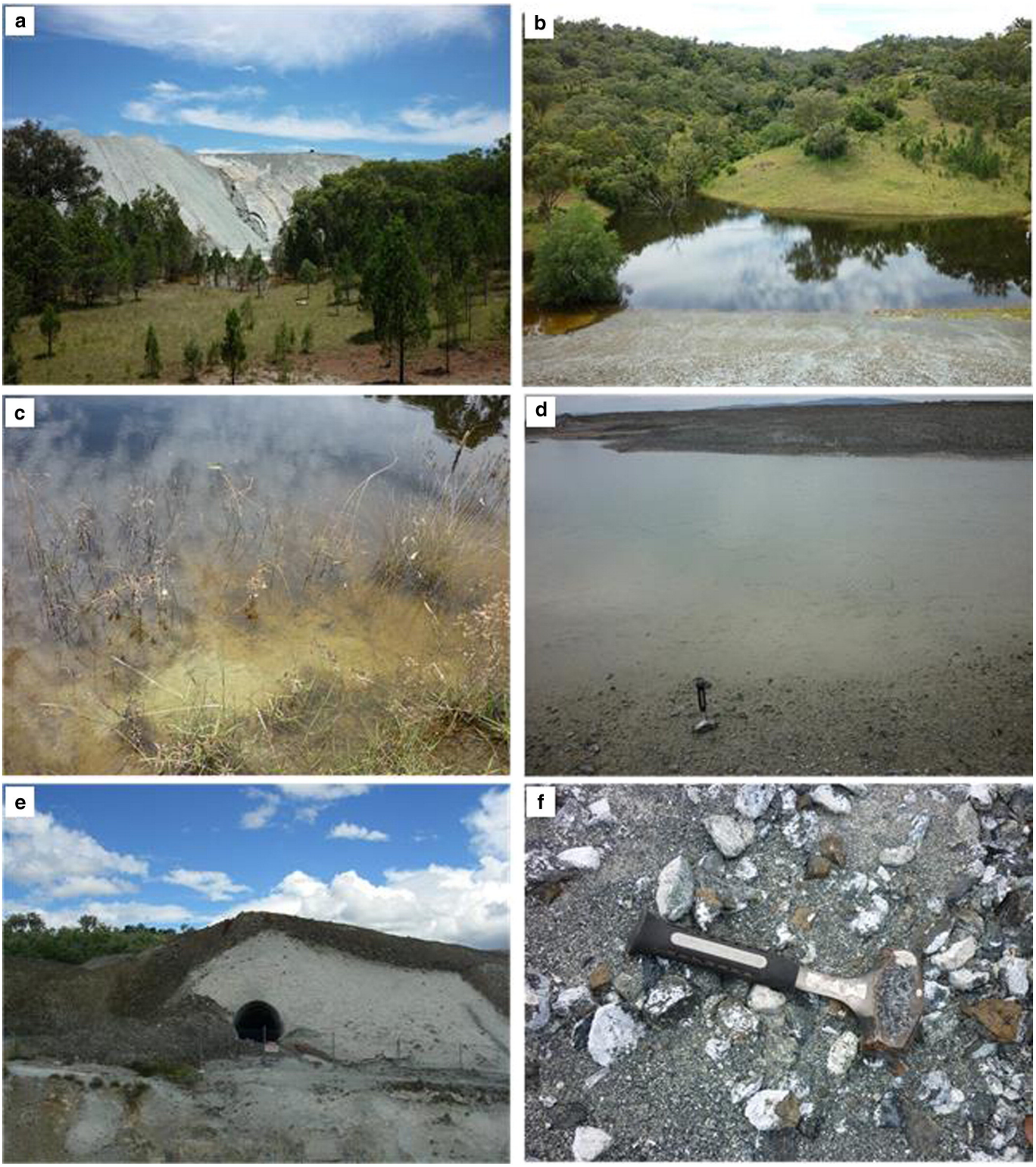

Fig. 2. Sampling locations of water and carbonate from Woodsreef tailings. a. View on tailings pile from south-east. b. Stream intersecting tailings (WO-P). c. Sediment at the bottom of pond shown in b. d. Water puddle in depression on top of tailings after rain-fall (WO-TOP). e. Entry to tunnel into tailings (WO-TU). f. Cobble coatings at south-eastern base of tailings (WO-CC).

$$[CO_2{*}] = [CO_{2aq}] + [H_2CO_3]. \quad (2)$$

The equilibrium between gaseous CO_2 and $[CO_2{}^*]$ can be described by Henry's law based on the fugacity of gaseous CO_2 ($f(CO_2)$) and the solubility coefficient of CO_2 in water (K_0):

$$[CO_2{*}] = f(CO_2) \times K_0. \quad (3)$$

Because of the small difference between the fugacity and the partial pressure of CO_2 (i.e.,<1%; Dickson et al., 2007; Zeebe, 2012), Eq. (3) can

be simplified to

$$pCO_2 \approx f(CO_2). \quad (4)$$

The fugacity of CO_2 ($f(CO_2)$) is calculated in PHREEQC based on measured values for temperature, pH and DIC concentration. Following computation of speciation, including [CO_2*], waters are equilibrated with atmospheric pCO_2 of 390 μatm, affording the assessment of the resulting pH and DIC concentrations. Ratios of $pCO_{2sample}/pCO_{2atmosphere}$ and of $DIC_{measured}/DIC_{equilibrium\ with\ atmosphere}$ are used to assess the degree of equilibration of water with the atmosphere as well as the tendency to absorb or degas CO_2, as indicated by ratios <1 and <1, respectively. While the pCO_2 of a water provides a measure of the thermodynamic driving force of CO_2 exchange between fluid and atmosphere, the rate of CO_2 exchange strongly depends on the convective mass transfer coefficient, which in the case of small headwater streams is a function of water turbulence at the gas-water interface (Butman and Raymond, 2011; Zappa et al., 2007).

The fraction of remaining liquid (f) can be calculated using a Rayleigh-type distillation related to the evaporative loss of fluid in combination with a humidity-dependent kinetic fractionation for stable O and H isotopes, based on the following equation by Gonfiantini (1986):

$$f = \exp\left[\left(\delta^{18}O^{i}_{H_2O(l)} - \delta^{18}O^{r}_{H_2O(l)}\right) \times \left(\varepsilon_{H_2O(l)-H_2O(g)} + \Delta\varepsilon_{H_2O(l)-H_2O(g)}\right)^{-1}\right]. \quad (5)$$

The terms $\delta^{18}O^{i}_{H_2O(l)}$ and $\delta^{18}O^{r}_{H_2O(l)}$ describe the initial and the resulting isotopic composition of the fluid, respectively. Two linear trend lines fitted through the groups of stream and meteoric water samples intersect the LMWL at $\delta^{18}O = -4.4$ ($\delta^{2}H = -24.7$), which we use as the best available estimate of the initial isotopic composition of the fluids, $\delta^{18}O^{i}_{H_2O(l)}$, while the measured $\delta^{18}O$ is used as the resulting isotopic composition, $\delta^{18}O^{r}_{H_2O(l)}$. For the equilibrium and kinetic fractionation terms, $\varepsilon_{H_2O(l)-H_2O(g)}$ and $\Delta\varepsilon_{H_2O(l)-H_2O(g)}$, we use the temperature dependent fractionation factors of Kakiuchi and Matsuo (1979) at temperatures determined in the field and the kinetic fractionation factors of Gonfiantini (1986), respectively. Average relative humidities measured at the nearest weather station at Barraba ranged between 38% and 88% (Australian Government Bureau of Meteorology). The calculated change in $\delta^{2}H$ and $\delta^{18}O$ with increasing evaporation based on Eq. (1) and the fractionation factors of Kakiuchi and Matsuo (1979) and Gonfiantini (1986) is shown in Table 4.

4. Results and discussion

4.1. Chemistry of water samples

To discuss the interactions of natural waters with the tailings material, we split the samples into two genetically related groups, with stream waters WO-US, WO-P, WO-DS and meteoric waters MWT, WO-TOP, WO-TU depicted as diamonds and circles in diagrams, respectively. Field parameters pH, temperature and conductivity as well as cation concentrations and isotopic compositions are shown in Table 2.

The measured temperatures reflect warm air temperatures during the sampling campaign but also the sampling context, with the stagnant waters WO-TOP and WO-P being significantly warmer than flowing waters and the drip water from the tunnel. Conductivities range between 150 and 1000 μS/cm and a positive correlation exists between the conductivity and the DIC concentration of waters in both sample groups (stream and meteoric water, Fig. 3a). The DIC constitutes around 50 wt.% of the total dissolved solids, suggesting that other anions play only a minor role in the chemistry of the waters at Woodsreef. This is confirmed by low concentrations of chloride, sulfate and nitrate relative to DIC observed in a previous study of waters from Woodsreef (Toyer and Main, 1978).

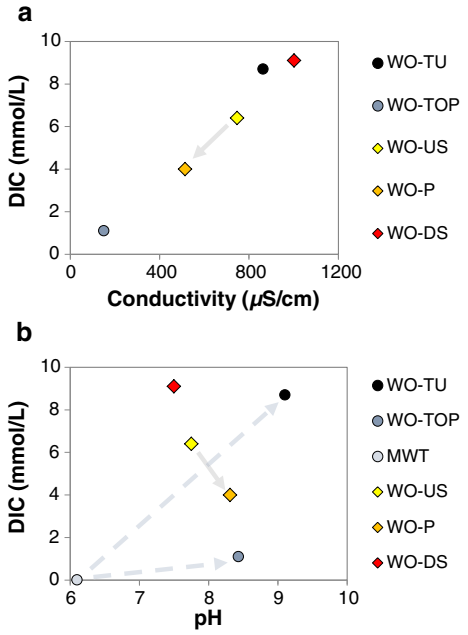

Fig. 3. a. Relationship between DIC concentration and conductivity. b. Relationship between DIC and pH of the sampled waters. Meteoric and stream water samples are depicted as circles and diamonds, respectively. Solid and dashed arrows indicate inferred genetic relationships between stream and meteoric waters, respectively.

The pH of water samples ranges from 6.1 for the water tank sample, between 7 and 8.3 for stream water samples and between 8.4 to 9.1 for samples from the puddle on the tailings and drip water in the tunnel. The pH of 6.1 of MWT is slightly higher than expected for equilibrium with atmospheric CO_2 (i.e., pH = 5.8), likely reflecting chemical reactions with windblown material and microorganisms in the water tank environment. Stream waters display a negative relation between pH and DIC concentration (Fig. 3b), consistent with either increasing pH due to degassing or acidification by uptake of carbonic acid. The pCO_2 (partial CO_2 pressure of a hypothetical atmosphere in equilibrium with water) of the stream waters is between 1200 and 22,400 μatm, which are thus prone to degas CO_2 upon equilibration with atmospheric CO_2. Similar pCO_2 has been observed in other streams in carbonate dominated catchments, e.g. the Wiesent River in Germany (Doctor et al., 2008; van Geldern et al., 2015). The pH and DIC of meteoric waters are positively correlated, with higher DIC coinciding with higher pH. This indicates a distinct evolution of the carbonate system in these samples, which is likely dominated by dissolution–precipitation processes. The pCO_2 of meteoric waters WO-TU and WO-TOP is slightly lower than atmospheric pCO_2 (ratio of $pCO_{2sample}/pCO_{2atmosphere}$ of 0.77 and 0.72, respectively) and consequently this group of samples will absorb CO_2 upon equilibration with the atmosphere. The pH of a drip water left open to the tunnel atmosphere decreased from 9.1 to 8.9 within 2.5 h.

The main cations in the water samples comprise Mg, Ca, Si, Na and K, with Fe and Al only present in MWT and Ag, As, B, Be, Cd, Cr, Co, Cu, Mn, Ni, Pb, Sn, Sr, Tl, being below the detection limit of about 50 ppb. The group of stream waters (WO-US, WO-P and WO-DS) are chemically distinct in that they contain up to 85, 24 and 29 ppm of Ca, Si and Na, respectively, whereas these elements do not exceed 2 ppm in the meteoric-derived group (WO-TU, WO-TOP and MWT), illustrating the contribution of country rock dissolution to the cation budget of the former group.

4.2. Carbonate samples

Table 3 assembles the mineralogical composition of the solid samples associated with the studied water specimens and X-ray diffractograms are shown in the supplement (Figs. S1 to S4 in the online version at http://dx.doi.org/10.1016/j.chemgeo.2016.04.014.). The bulk samples consist predominantly of the serpentine polymorph lizardite (and chrysotile remaining after processing) but the carbonate minerals pyroaurite and hydromagnesite are also abundant. The textural context of sample WO-TU$_s$ at the discharge point of the drip water indicates a genetic relationship between the dripwater and the hydromagnesite component of the sample, i.e. the hydromagnesite has precipitated from a solution similar to WO-TU.

WO-MFB, a sample from a depression on top of the tailings pile, also bears a close genetic relationship to the water sample WO-TOP, however, the interaction of the water with the tailings material is in this case restricted by a low permeability layer forming the base of the depression. This impermeable layer is best represented by sample WO-MFB but also by other horizontal crusts investigated in Oskierski et al. (2013a). The formation of relatively impermeable carbonate crusts has been observed on other ultramafic tailings piles, e.g., at the Mount Keith Nickel mine and has been ascribed to efflorescence of carbonate minerals (Wilson et al., 2014). In some instances, the edges of the depressions on top of the tailings reveal a fine lamination, which could potentially reflect formation during repeated cycles of sedimentation from stagnant water after rainfall events. While the sampling context on top of the tailings and the presence of calcite may suggest addition of windblown calcite with a marine limestone carbon isotope signature ($\delta^{13}C = -1$ to 1), the lower $\delta^{13}C$ of WO-MFB results either from the addition of carbonate with a low bedrock-magnesite isotope signature during mining and deposition of the tailings or from kinetic isotope effects during uptake of CO_2 into solution (Wilson et al., 2010).

Larger, cm-sized cobbles of serpentinite rock are often partly coated with white carbonate crusts. The coatings preferentially form on the underside of the cobbles suggesting that extended periods of moisture promote their formation (Wilson et al., 2009). Coated cobbles could potentially be a result of the formation of vertical crusts and spires (see Fig. 2b in Oskierski et al., 2013a) on the tailings pile and their downward transport on the eroding slope. However, their predominant occurrence along the south-eastern bottom edge of the pile coincides with a series of silting ponds (and the water flowing between them) and thus suggests a genetic relationship to process waters.

4.3. Isotopic fingerprints

4.3.1. Stable carbon isotope signatures of dissolved inorganic carbon (DIC)

The stable isotopic signature of DIC and carbonates can be used as a fingerprint to trace the sources of carbon in a water sample. Potential sources of carbon in the mine tailings are organic material/soil, bedrock carbonate (predominantly magnesite), windblown carbonate dust and atmospheric CO_2, each with a distinct carbon isotopic signature. Considering equilibrium fractionation of carbon isotopes during dissolution of soil CO_2 and atmospheric CO_2, fields for DIC derived from the potential carbon sources in the mine tailings can be established based on published fractionation factors and their extrapolation to surface temperatures between 0 and 40 °C prevalent at Woodsreef (i.e., $\varepsilon_{CO2(g)-HCO3-}$ of Mook et al. (1974)). Since bicarbonate is the dominant ion in the pH range of the studied water samples (between 85 and 97% of DIC), we use the fractionation factors of bicarbonate to approximate the isotopic composition of the DIC in our calculations. For organic material/soil, bedrock magnesite and windblown carbonate dust, we use $\delta^{13}C_{OM}$ of −27 to −22‰, $\delta^{13}C_{magnesite}$ of −12.9 to −11.4‰, $\delta^{13}C_{limestone}$ of −1 to 1‰ and $\delta^{13}C_{CO2}$ in air of −9 to −7‰, respectively, taken from a previous study of isotopic signatures at Woodsreef (Oskierski et al., 2013a) and from Clark and Fritz (1997).

DIC in stream waters is commonly derived from soil CO_2 or dissolution of bedrock carbonate, and the contribution from these carbon reservoirs can be quantified based on their distinct isotopic signature (Clark and Fritz, 1997; Doctor et al., 2008; van Geldern et al., 2015). At Woodsreef, however, weathering-derived bedrock magnesite, a typical low temperature alteration product of serpentinite, has significantly lower $\delta^{13}C$ than marine limestone, leading to overlapping isotopic fingerprints for DIC derived from soil CO_2 and dissolution of bedrock magnesite (Fig. 4). Another overlap exists between the $\delta^{13}C_{DIC}$ derived from atmospheric CO_2 and the dissolution of calcite with a typical marine limestone isotope signature.

Since the stream has not flowed through any ultramafic lithologies and is sampled before it enters the Woodsreef serpentinite, it is unlikely that any of the carbon in sample WO-US is derived from bedrock magnesite. The $\delta^{13}C_{DIC}$ of sample WO-US thus reflects carbon derived

Table 3
Mineralogical and isotopic composition of solid samples.

Sample	WO-TU$_s$	WO-MFB[a]	WO-FC	WO-CC
Context and mode	Crust at discharge point of drip water	Sediment in depression on tailings	Sediment from ephemeral stream	Cobble coating
Coordinates	−30.407788	−30.411253	−30.411181	−30.415168
	150.739534	150.740536	150.736715	150.741306
Lizardite	**	****	****	**
Chrysotile[b]	*	*	*	*
Magnetite		*	*	*
Forsterite			*	*
Brucite		*		*
Diopside		*		
Pyroaurite	**	*	**	**
Hydromagnesite	***	*	*	***
Calcite		****		
Magnesite			*	
Quartz	*	**	*	
$\delta^{13}C_{graphite}$ (‰,VPDB) (1σ)	1.6 (0.2)	−4.2 (0.1)	2.1 (0.1)	n.d.
pMC (%) (1σ)[c]	111.75 (0.39)	92.6 (0.36)	112.13 (0.31)	n.d.
Conventional radiocarbon age (yBP)	Modern	615 ± 35	Modern	n.d.
$\delta^{13}C_{carbonate}$ (‰,VPDB) (1σ)	3.2 (0.05)	−5.8 (0.05)	2.3 (0.05)	n.d.
$\delta^{18}O_{carbonate}$ (‰,VSMOW) (1σ)	33.4 (0.09)	26.1 (0.09)	31.7 (0.09)	n.d.

****Predominant; ***subdominant; **abundant; *minor; *trace.
n.d. — not determined.
[a] Mineral abundances from Oskierski et al. (2013a).
[b] Abundance estimated relative to lizardite content.
[c] pMC = percent modern carbon.

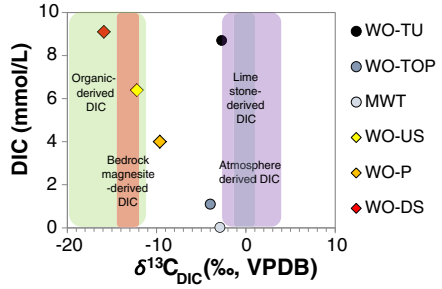

Fig. 4. DIC concentration plotted against $\delta^{13}C_{DIC}$; fields for DIC in equilibrium with organic carbon, bedrock carbonate and atmospheric CO_2.

from organic material or soil. Sample WO-P from a pond intersecting the tailings pile displays lower DIC concentration and higher $\delta^{13}C_{DIC}$ than WO-US, consistent with downstream degassing and precipitates observed in the pond. Sample WO-DS, a water re-emerging downstream of the tailings pile, has the highest DIC concentration and a very low $\delta^{13}C_{DIC}$ signature of −15.9‰ (Table 2), which indicates that either bedrock magnesite or organic material provides the carbon in this sample.

The stream water samples display a negative, near linear relationship between concentration and stable carbon isotopic composition of DIC (Fig. 4). This can be interpreted as a simple mixing line between carbon sources, i.e., atmospheric CO_2 and soil CO_2/bedrock magnesite, or as a result of CO_2 degassing and carbonate precipitation, gradually leading to lower DIC concentration and higher $\delta^{13}C_{DIC}$ (Bar-Matthews et al., 1996). A similar interpretation can be derived from Fig. 5 that affords a correlation between $\delta^{13}C_{DIC}$ and the $pCO_{2sample}/pCO_{2atmosphere}$ ratio. Stream waters approach the theoretical $\delta^{13}C_{DIC}$ of 0.3‰ for a ratio of 1 (100% equilibration with atmospheric CO_2), calculated at 25 °C using $\delta^{13}C_{CO2}$ of −7.6‰ (Friedli et al., 1986) and fractionation factors of Mook et al. (1974), consistent with the above interpretation.

Compared to the stream waters, the rainwater sample MWT has a higher $\delta^{13}C_{DIC}$ which, however, is slightly lower than expected for DIC in equilibrium with atmospheric CO_2 (Fig. 4). Sample WO-TOP from the top of the tailings pile displays higher DIC concentration and lower $\delta^{13}C$ than MWT, indicating that, carbon in this sample is predominantly derived from atmospheric CO_2, with potential contributions from the dissolution of bedrock or windblown marine carbonate. The $\delta^{13}C_{DIC}$ of the tunnel drip water WO-TU is similar to that of MWT, suggesting carbon of atmospheric origin but WO-TU displays significantly higher DIC concentration. The sampling context and evolution of meteoric-derived waters suggests that they contain predominantly atmospheric-derived CO_2. Lower than expected $\delta^{13}C_{DIC}$ in meteoric-derived waters could thus be explained as a result of kinetic isotope fractionation during uptake of CO_2 into solution (Wilson et al., 2010) or the precipitation of carbonate, preferentially removing ^{13}C.

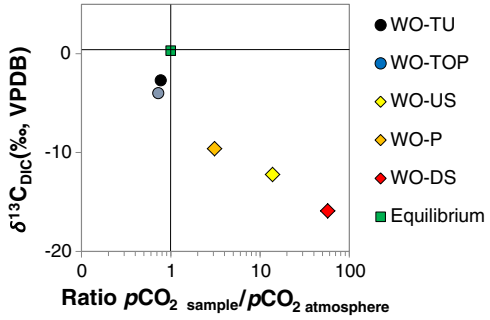

Fig. 5. $\delta^{13}C_{DIC}$ plotted against $pCO_{2sample}/pCO_{2atmosphere}$.

The meteoric-derived waters WO-TOP and MWT appear to represent a continuation of the trend displayed by the stream waters in Fig. 4, representing the atmospheric endmember of a two component system. Drip water WO-TU, on the other hand, is characterised by significantly higher DIC concentrations of 8.7 mmol/L at similar $\delta^{13}C_{DIC}$ as the genetically related rainwater MWT. While the DIC concentration of meteoric water samples WO-TOP and WO-TU is close to equilibrium with atmospheric CO_2 ($DIC_{measured}/DIC_{equilibrium\ with\ atmosphere}$ of 0.99 and 0.98, respectively), $pCO_{2sample}/pCO_{2atmosphere}$ ratios of 0.77 and 0.72, respectively, document the tendency of these samples to absorb atmospheric CO_2. This demonstrates that the meteoric-derived waters approach theoretical equilibrium $\delta^{13}C_{DIC}$ on a different pathway than the stream waters, including a concomitant increase in DIC concentration and pH via uptake of atmospheric CO_2 and dissolution-derived alkalisation, respectively.

4.3.2. Radiocarbon content of dissolved inorganic carbon (DIC)

Due to the overlap of carbon isotopic signatures of different carbon sources, interpretation of $\delta^{13}C$ is not always unequivocal (Kralik et al., 1989; Oskierski et al., 2013a; Wilson et al., 2009). Some of the ambiguity in $\delta^{13}C$ can be resolved based on radiocarbon, which serves as a robust tracer for atmospheric CO_2, due to the almost exclusive production of ^{14}C in the upper atmosphere (Oskierski et al., 2013a; Wilson et al., 2009; Wilson et al., 2014). In a cross plot of $\delta^{13}C$ and $F^{14}C$ (Fig. 6), fields of carbon source fingerprints are effectively separated, enabling unequivocal identification of carbon sources. The high radiocarbon content of sample WO-TU (and MWT) clearly demonstrates that, DIC in these samples is derived from atmospheric CO_2 and not from dissolution of limestone.

4.3.3. Isotope signatures of solid samples

Carbonate precipitate WO-TU_s, formed at the discharge point of WO-TU, also displays a clear atmospheric carbon isotope signature with $\delta^{13}C$ of 3.2‰ and $F^{14}C = 1.11$, as expected for formation in isotopic exchange equilibrium with atmospheric CO_2. The same is true for the cobble coating WO-CC, whereas WO-MFB, the sediment sample from the depression on top of the tailings, has a lower $\delta^{13}C$ and $F^{14}C$ fingerprint, indicating contribution of a non-atmospheric carbon source. Both $\delta^{13}C$ and $\delta^{18}O$ signatures of WO-TU and WO-CC are in accordance with signatures observed for vertical carbonate crusts forming elsewhere on the tailings pile, while the isotopic fingerprint of WO-MFB concurs with that of other horizontal crusts on the Woodsreef tailings (Oskierski et al., 2013a).

Even though the bulk sample WO-TU used for mineral identification by XRD is a mixture of different minerals, the contribution of pyroaurite to the isotopic signature is likely negligible because of the distinct formation mechanism inferred for pyroaurite and selective sampling for IRMS targeting hydromagnesite. Therefore, we use the genetic relationship between the dripwater WO-TU and the precipitate WO-TU_s to assess the isotopic fractionation between water and hydromagnesite.

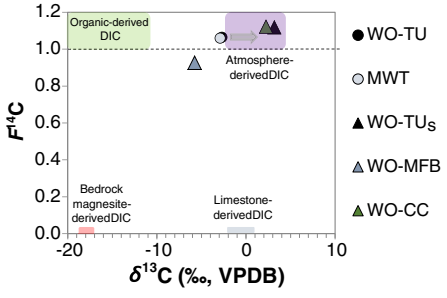

Fig. 6. Carbon isotopic signatures ($F^{14}C$ and $\delta^{13}C$) of DIC and carbonate samples. Fields for DIC with different sources of CO_2. The arrow indicates isotopic fractionation expected for precipitation of hydrated Mg-carbonate (Wilson et al., 2010); note that sample WO-TU plots behind MWT.

The observed empirical isotope fractionation is $\Delta^{13}C_{Hmgs\text{-}DIC} = 5.9 \pm 0.2‰$ and $\Delta^{18}O_{Hmgs\text{-}H2O} = 37.6 \pm 0.2‰$, for water sampled at 17.2 °C. Due to the contamination by calcite, the isotopic fingerprint of solid sample WO-MFB cannot be used to constrain fractionation between the genetically related fluid and hydromagnesite.

4.3.4. Hydrogen and oxygen isotope signatures of water

Evaporation is considered a key process in the carbonation of ultramafic mine tailings (Oskierski et al., 2013a; Wilson et al., 2014). Fig.7 shows the hydrogen and oxygen isotopic composition of water samples from the study site relative to the global meteoric water line (GMWL, Craig, 1961), a local meteoric water line (LMWL), as well as a local evaporation line (LEL, Andersen et al., 2008).

The LMWL, running parallel but slightly above the GMWL, is based on rain-water samples collected in the Namoi River catchment about 50 km west of Woodsreef, with (co-)variability in δ^2H and $\delta^{18}O$ resulting from variations in moisture source areas, transport paths and precipitation histories (Andersen et al., 2008; Munksgaard et al., 2012). While meteoric water samples of Andersen et al. (2008) plot along the LMWL, surface waters from the Namoi River catchment define an evaporative trend, expressed as the LEL in Fig. 7, with local groundwater samples clustering around the intersection of LMWL and LEL (Andersen et al., 2008). The isotopic composition of evaporated samples is shifted from the LMWL towards the LEL because kinetic isotope fractionation during evaporation affects oxygen more strongly than hydrogen.

Among the stream water samples from Woodsreef, WO-US plots only slightly below the LMWL, with less than 3% of water evaporated at the time of sampling, whereas 10 to 15% of WO-P have evaporated, consistent with the sampling context from a stagnant pond at the base of the tailings. Based on the expected flow path of the stream, sample WO-DS could be interpreted as derived from stream waters WO-US and WO-P (Fig. 1c). However, the hydrogen and oxygen isotopic composition of WO-DS plots on the LMWL, indicating insignificant evaporation of less than 1% and thus that WO-DS is not directly related to the more evaporated sample WO-P.

In the group of meteoric-derived samples, MWT has undergone 2 to 4% evaporation, whereas the hydrogen and oxygen isotope composition of WO-TU and WO-TOP are slightly below the LMWL and the LEL, respectively. This indicates incipient evaporation of drip water sample WO-TU (1 to 2%), whereas WO-TOP has undergone significant evaporation of 7 to 11% at the time of sampling, in accordance with the sampling context from a puddle on top of the tailings. For sample WO-TU, we calculate a theoretical oxygen isotopic composition based on the equilibrium fractionation factor $\delta^{18}O_{hydromagnesite\text{-}H2O(l)}$ from O'Neil and Barnes (1971) and the isotopic signature of carbonate precipitate WO-TU_s. This demonstrates that WO-TU_s has precipitated from a solution that was at least 13 to 20% evaporated (Table 4). Evaporation of fluids is also suggested by the relatively high $\delta^{18}O$ signatures of the solid carbonate samples (Kralik et al., 1989).

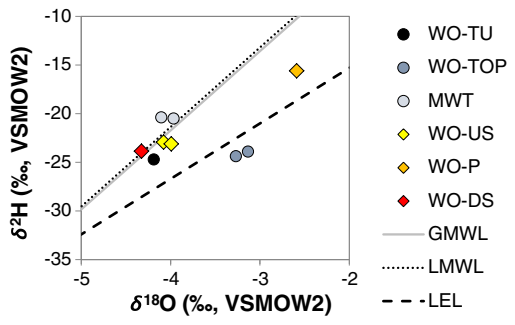

Fig. 7. Cross plot of the hydrogen and oxygen isotopic composition of water samples form Woodsreef; global meteoric water line (GMWL), local meteoric water line (LMWL) and a local evaporation line (LEL) from Andersen et al. (2008), shown as straight, doted and dashed lines, respectively.

4.4. Evolution of stream water

Elevated concentrations of Ca, Si and Na reflect the interaction with the country rocks of the Woolomin Group to the east of the Woodsreef serpentinite, while low $\delta^{13}C_{DIC}$ indicates soil-derived CO_2 as the dominant carbon source in stream water WO-US. Due to relatively high DIC concentrations (6.4 mmol/L) and pCO_2 (5370 µatm), the sample is prone to degas when in contact with atmospheric CO_2. Degassing of CO_2, which occurs in 95% of inland streams and rivers globally (Raymond et al., 2013), is commonly accompanied by increased $\delta^{13}C_{DIC}$, pH and carbonate supersaturation in downstream samples (Bar-Matthews et al., 1996; Doctor et al., 2008; Fairchild et al., 2006; Gray et al., 2011; Holland et al., 1964; Polsenaere and Abril, 2012; van Geldern et al., 2015).

Sample WO-P, taken from a pond at the base of the tailings, exhibits lower DIC concentration and pCO_2, higher pH and higher $\delta^{13}C_{DIC}$ than WO-US. Despite significant evaporation evidenced by δ^2H and $\delta^{18}O$ signatures, cation concentrations in WO-P are lower than in WO-US, indicating that cations have been removed by precipitation. This is consistent with an increase of pH, driven both by contact with the alkaline Woodsreef serpentinite and degassing of CO_2.

Table SI 1 in the online version at http://dx.doi.org/10.1016/j.chemgeo.2016.04.014. shows the progression of saturation indices as predicted by our thermodynamic PHREEQC model. A water similar to WO-US dissolves brucite, warms to ambient temperature, evaporates (18% evaporation), degasses CO_2 and precipitates selective minerals, such as hydromagnesite and calcite. The results are illustrative because dissolution and precipitation of solid phases will be governed by kinetic as well as thermodynamic constraints. However, it is demonstrated that the envisaged evolution significantly increases saturation and that a solution equivalent to WO-P can form.

The evolution of stream water WO-DS is more difficult to constrain as the relationship to the other stream waters is somewhat obscure. The low degree of evaporation indicates that WO-DS, even though downstream of WO-P, has been recharged from other, non-evaporated sources. According to earlier assessments of flow paths, the stream water is flowing laterally along the saturated zone at the bottom of the tailings pile (see Fig. 1c; Svanosio, 2000; Toyer and Main, 1978) but potentially receives inputs from other stream tributaries, rain water or runoff. Upon emerging downstream of the tailings pile, WO-DS possesses less alkaline pH than the other water samples along with high DIC concentration and low $\delta^{13}C_{DIC}$ signature. In the absence of an obvious source of organic carbon within the saturated zone of the tailings, the chemical and isotopic composition of WO-DS most likely reflects dissolution of bedrock magnesite ($\delta^{13}C = -12.9$ to $-11.4‰$) and brucite, based on relatively fast dissolution rates (at pH = 7 and 25 °C) of both minerals compared to chrysotile and olivine (Bales and Morgan, 1985; Harrison et al., 2013; Pokrovsky and Schott, 2000; Pokrovsky and Schott, 2004; Pokrovsky et al., 2005), accompanied by minor serpentine dissolution producing the moderate Si-concentration of 23.6 mg/L in WO-DS. Alternatively, WO-DS might be more representative of a spring or ground water charged with soil CO_2, which is emerging freshly from the ultramafic bedrock. In their study of a karst system in semi-arid climate, Bar-Matthews et al. (1996) found that, waters containing DIC derived from soil CO_2 and bedrock carbonate evolve from high DIC concentration and low $\delta^{13}C_{DIC}$ signature to lower DIC and higher $\delta^{13}C_{DIC}$ via degassing and carbonate precipitation, following a broadly similar trend as stream waters at Woodsreef. The authors calculate a $\delta^{13}C_{DIC}$ of $-15.3‰$ for the initial isotopic composition of these waters based on a Rayleigh fractionation model (Bar-Matthews et al., 1996), which is consistent with the $\delta^{13}C_{DIC}$ of WO-DS ($\delta^{13}C_{DIC} = -159$ ‰). This suggests that, WO-DS could indeed be the least evolved sample in the group of stream waters.

Table 4
Calculated degree of evaporation, change in hydrogen and oxygen isotopic composition and associated hydromagnesite saturation during evaporation.

Sample	WO-TU	WO-TU (solid)[a]	WO-TOP	MWT	WO-US	WO-P	WO-DS
Degree of evaporation (%) (RH88)[b]	2	20	11	4	3	15	<1
Degree of evaporation (%) (RH38)[c]	1	13	7	2	2	10	<1
Saturation Index Hydromagnesite[d]	−0.77	−0.31[e]	−9.61	−42.94	−9.94	−7.04	−8.90
30% evaporation							
δ^2H_{water} (‰,VSMOW) (RH88)	3.8		5.2	1.2	3.7	2.7	3.8
δ^2H_{water} (‰,VSMOW) (RH38)	6.1		7.4	3.4	5.9	4.9	6.1
$\delta^{18}O_{water}$ (‰,VSMOW) (RH88)	−0.2		−0.5	−0.4	−0.3	−0.6	−0.3
$\delta^{18}O_{water}$ (‰,VSMOW) (RH38)	2.3		2.0	2.1	2.2	1.9	2.2
Saturation Index Hydromagnesite	−0.03		−8.49	−41.74	−8.94	−6.16	−8.25
50% evaporation							
δ^2H_{water} (‰,VSMOW) (RH88)	30.8		33.3	25.6	30.4	28.5	30.8
δ^2H_{water} (‰,VSMOW) (RH38)	35.1		37.6	29.9	34.7	32.9	35.1
$\delta^{18}O_{water}$ (‰,VSMOW) (RH88)	3.8		3.1	3.3	3.5	3.0	3.5
$\delta^{18}O_{water}$ (‰,VSMOW) (RH38)	8.7		8.0	8.2	8.4	7.9	8.4
Saturation Index Hydromagnesite	0.63		−7.51	−40.58	−8.04	−5.36	−7.87

[a] Calculated based on equilibrium fractionation between fluid and solid sample WO-TU$_s$ (see text).
[b] Relative humidity of 88%.
[c] Relative humidity of 38%.
[d] Calculated in PHREEQC based on measured sample composition.
[e] Calculated for 20% evaporation.

For both scenarios, i.e., interaction with tailings or bedrock, carbon is likely derived from both soil CO_2 and dissolution of bedrock carbonate, which cannot be discerned based on their stable carbon isotope signatures.

4.5. Evolution of meteoric derived water

Due to the sampling from a puddle on top of the tailings after a rainfall, WO-TOP can be easily identified as a meteoric-derived water. The incipient interaction of meteoric water with the tailings material is clearly reflected in increased pH, conductivity and cation concentrations of WO-TOP relative to MWT. Carbon isotopic signatures of both samples indicate dissolution of atmospheric CO_2 in rainwater, albeit with $\delta^{13}C_{DIC}$ values lower than expected for equilibrium with atmospheric CO_2. Carbonic acid derived from atmospheric CO_2 provides the acidity for initial dissolution of tailings material. Both waters are undersaturated with respect to the expected carbonate phases (see Tables 4 and SI 2 in the online version at http://dx.doi.org/10.1016/j.chemgeo.2016.04.014.).

Fluid flow and transport processes are considered to be predominantly vertical in the vadose zone and hence mine tailings are commonly conceptualised as a one-dimensional column (Bea et al., 2011). The sample WO-TU can thus be interpreted as a rainwater which infiltrates and reacts with the tailings material along a vertical flow path to emerge as a drip water in the tunnel below the tailings pile (Fig. 2e). During transport through the tailings the fluid evolves from a low salinity rain water with a pH around 6 into a Mg-rich, alkaline water with a pH of 9.1, indicating dissolution of tailings material. Together with the increased DIC concentration, this could be interpreted as the dissolution of bedrock carbonate minerals, a scenario in which no net-carbon sequestration would be achieved due to the lack of a non-carbonate Mg-source (Wilson et al., 2009). However, the high $\delta^{13}C_{DIC}$ of −2.7‰ as well as the $F^{14}C_{DIC}$ of 1.06 preclude bedrock magnesite as the dominant source of carbon in sample WO-TU. Instead our calculations demonstrate, that pCO_2 in WO-TU is lower than pCO_2 of the tunnel atmosphere, resulting in absorption of CO_2 into the solution, despite relatively high DIC concentration. This has been confirmed by observing the pH of WO-TU decrease over time when left open to the tunnel atmosphere (i.e., 0.2 pH units within 2.5 h). Table SI 2 in the online version at http://dx.doi.org/10.1016/j.chemgeo.2016.04.014. illustrates a possible pathway for the evolution of rain water MWT into WO-TU, including open and closed system dissolution of tailings minerals, uptake of CO_2 into the solution as well as evaporation.

Due to the relatively low flow and drip rate, sample WO-TU has time to equilibrate with atmospheric CO_2 during both the final portion of the flow path and during sampling. Consequently, some of the direct information on the interaction between water and tailings minerals may have been overprinted and the clearly atmospheric isotopic signatures indeed reflect the uptake of atmospheric CO_2 into a high-pH water, occurring after the solution was alkalised by dissolution of tailings material. In this scenario, DIC is predominantly derived from the ingress of CO_2 from the tunnel atmosphere while Mg is derived from a non-carbonate source. The low Si concentration of WO-TU suggests that, only relatively little serpentine has been dissolved (i.e. 0.00015 mol chrysotile per kg of water, according to our model), in accordance with results for the carbonation of other mine tailings, e.g., the Mt. Keith Nickel mine (Harrison et al., 2013; Wilson et al., 2014). Alternatively, precipitation of amorphous silica (or quartz) has removed Si from the fluid, consistent with the presence of these phases in the tailings pile (Oskierski et al., 2013a). Phases formed during incipient weathering of minerals in serpentinite commonly display lower Mg/Si ratios than precursor minerals, suggesting incongruent release of Mg during replacement (Oskierski, 2013), which could contribute to the formation of high-Mg, low-Si fluids. Incongruent dissolution of serpentine minerals is considered to result from initially faster dissolution of the less strongly bound Mg^{2+} ions in the outer brucite sheets in the structure of serpentine minerals leaving behind the less reactive siloxane sheets (Bales and Morgan, 1985; Park and Fan, 2004). However, the incongruent release of Mg could also be interpreted as a result of coupled stoichiometric dissolution and reprecipitation of silica (Putnis, 2009). Due to the relatively short reaction time between water and tailings, it is instead likely that, a large proportion of Mg is derived from the dissolution of brucite, a minor but highly reactive phase present in the mine tailings, which has been considered to contribute significantly to alkalisation of the fluids and the carbonation potential of ultramafic tailings and rocks (Assima et al., 2013b; Bea et al., 2011; Beinlich and Austrheim, 2012; Harrison et al., 2013; Pronost et al., 2011; Wilson et al., 2014).

4.6. Open and closed system evolution

Reactive transport models are commonly used to describe the interaction of waters with ultramafic rocks (Bea et al., 2011; Bruni et al., 2002). Availability of gaseous CO_2, i.e., open or closed system behaviour with respect to CO_2, has been identified as crucial for the evolution of alkaline spring waters in contact with ultramafic rocks, which evolve from moderate pH, Mg–HCO_3 dominated to high pH, Ca–OH dominated

waters under open and closed system conditions, respectively (Bruni et al., 2002; Cipolli et al., 2004; Marques et al., 2008; Paukert et al., 2012). In this context, stream water WO-DS would classify as a moderately alkaline, Mg–HCO_3 dominated water, suggesting access of soil CO_2 along the flow path at the bottom of the tailings. This is also consistent with the high DIC concentration and pCO_2 of WO-DS, which for groundwater is commonly a result of carbonate dissolution under constant supply of carbonic acid under open system conditions (Clark and Fritz, 1997; van Geldern et al., 2015).

Drip water WO-TU possesses higher pH than WO-DS and a pCO_2 below that of the atmosphere, suggesting that WO-TU has partly evolved in a closed system with respect to atmospheric CO_2. The uptake of atmospheric CO_2 into the drip water WO-TU upon discharge into the tunnel demonstrates that, (1) pCO_2 within the tailings is below atmospheric pCO_2 and/or (2) uptake of CO_2 into alkaline solution is kinetically hindered, i.e., the uptake of CO_2 lags behind the alkalisation of the solution, as suggested by previous studies (Beinlich and Austrheim, 2012; Clark et al., 1992; O'Neil and Barnes, 1971; Wilson et al., 2010). The former is corroborated by the presence of carbonate crusts on the outside of the tailings, which limit CO_2 ingress of atmospheric CO_2 at depth (Bea et al., 2011; Oskierski et al., 2013a; Wilson et al., 2014). The decrease of CO_2 concentrations with depth has also been confirmed by in-situ gas measurements in experimental mine tailings piles (Gras et al., 2015; Lechat et al., 2015; Lechat et al., 2016). The high degree of DIC equilibration ($DIC_{measured}/DIC_{equilibrium\ with\ atmosphere} > 0.98$) of meteoric-derived waters in combination with the relative large deviations of $\delta^{13}C_{DIC}$ from the equilibrium isotopic composition (3.0‰ for WO-TU, Fig. 5) also suggests kinetic isotope fractionation during uptake of CO_2 into water. The unexpectedly low $\delta^{13}C$ of sample WO-DS is consistent with kinetic isotope fractionation between atmospheric CO_2 and DIC ($\Delta^{13}C_{DIC\text{-}CO2} = -11.2$‰; O'Neil and Barnes, 1971; Wilson et al., 2010) but the high pCO_2 precludes atmospheric CO_2 as the main carbon source in sample WO-DS.

4.7. Isotope fractionation during precipitation

The $\delta^{13}C_{DIC}$ of water sample WO-TOP as well as $\delta^{13}C$ and $F^{14}C$ of the associated sediment sample WO-MFB are lower than expected for equilibrium with atmospheric CO_2. While this may be a result of kinetic carbon-isotope fractionation during uptake of CO_2 for WO-TOP, precipitation of hydrous Mg-carbonates occurs under equilibrium conditions (Beinlich and Austrheim, 2012; Wilson et al., 2010). Consequently, lower $\delta^{13}C$ in solid sample WO-MFB than in WO-TOP cannot be explained by isotopic fractionation during precipitation. The $\delta^{13}C$ of WO-MFB is in line with the isotopic signatures of other horizontal carbonate-rich crusts throughout the Woodsreef tailings, which display the addition of carbon from bedrock carbonate (Oskierski et al., 2013a). While the sampling context on top of the tailings and the presence of calcite may suggest addition of windblown calcite with a marine limestone carbon isotope signature ($\delta^{13}C = -1$ to 1), the lower $\delta^{13}C$ of WO-MFB results either from the addition of carbonate with a low bedrock-magnesite isotope signature during mining and deposition of the tailings or from kinetic isotope effects during uptake of CO_2 into solution (Wilson et al., 2010). This complexity precludes the evaluation of carbon or oxygen isotope fractionation between WO-TOP and WO-MFB.

The isotopic signatures of the solid, hydromagnesite-rich sample WO-TU_s are consistent with the ingress of atmospheric CO_2 into an alkaline solution. At the time of sampling, WO-TU is supersaturated with respect to Mg-rich carbonate phases, i.e., dolomite, huntite and magnesite, but due to the kinetic inhibition of precipitation of dolomite and magnesite precipitation at low temperatures (Arvidson and MacKenzie, 1999; Giammar et al., 2005; Hänchen et al., 2008; Saldi et al., 2009), hydrated Mg-carbonates, such as the observed hydromagnesite, precipitate preferentially. Bruni et al. (2002) argue that, the absorption of CO_2 into alkaline, Ca–OH waters, results in precipitation of calcite at the discharge point of ultramafic hosted springs. This is possible because, the highly evolved Ca–OH waters are depleted in DIC due to carbonate precipitation along their flow path (Bruni et al., 2002). Our calculations for WO-TU, however, indicate that, the uptake of CO_2 upon equilibration with atmospheric CO_2 does increase DIC concentration but reduces carbonate supersaturation due to the associated decrease in pH.

Based on the genetic relationship between water WO-TU and precipitate WO-TU_s and assuming hydromagnesite being the dominant carbonate phase in the subsample for isotopic analysis, the fractionation for carbon and oxygen isotopes can be determined as $\Delta^{13}C_{Hmgs\text{-}DIC} = 5.9 \pm 0.2$‰ and $\Delta^{18}O_{Hmgs\text{-}H2O} = 37.6 \pm 0.2$‰, respectively. Both carbon and oxygen isotope fractionation observed at Woodsreef are higher than the currently available estimates of equilibrium carbon isotope fractionation between DIC and hydrated Mg-carbonates, i.e., experimentally determined fractionation between DIC and dypingite ($Mg_5(CO_3)_4(OH)_2 \cdot 5H_2O$) of 3.8 ± 1.1‰ at 20 and 24.5 °C (Wilson et al., 2010) and of equilibrium oxygen isotope fractionation between water and hydromagnesite of 31.2‰ at 25 °C (O'Neil and Barnes, 1971).

5. Conclusions

As demonstrated by their chemical and isotopic signatures, stream waters and meteoric-derived waters interacting with the tailings at Woodsreef clearly evolve differently, enabling insight into two distinct pathways for carbonation. Stream waters are generally charged with soil-derived CO_2, with low $\delta^{13}C$, leading to pCO_2 which is significantly elevated above atmospheric levels (pCO_2 of 1200 to 22,390 μatm). Dissolution of country rock, ultramafic bedrock and/or tailings including bedrock magnesite occurs in an open system with respect to gaseous soil CO_2 enabling pCO_2 of the stream water to increase to more than 57 times the atmospheric pCO_2, providing a strong driving force for degassing. Degassing upon equilibration with atmospheric CO_2 out of contact with soil and bedrock magnesite increases pH and carbonate saturation, and eventually leads to carbonate precipitation, analogues to the formation of tufa and some speleothem deposits (Bar-Matthews et al., 1996; Fairchild et al., 2006; Holland et al., 1964). This evolution is reflected in negative correlations between DIC concentration and pH, as well as DIC concentration and $\delta^{13}C_{DIC}$ (Figs. 3b, 4). Despite the chemical driving force resulting from excess pCO_2, only moderate amounts of pyroaurite and traces of hydromagnesite are present in sediment sample WO-FC taken downstream from WO-DS, the sample exhibiting the highest pCO_2. This is likely due to the proximity to the discharge point, at which degassing has not progressed far enough to induce more significant carbonate precipitation, as well as to the low degree of evaporation that the water has undergone at this stage. Fluid alkalisation due to dissolution of tailings minerals and evaporation further increase carbonate saturation indices (see Tables SI 1 and 4 in the online version at http://dx.doi.org/10.1016/j.chemgeo.2016.04.014., respectively) and promote precipitation from pond water sample WO-P.

Despite the addition of some bedrock-derived carbon in WO-TOP and kinetic isotope effects during uptake of CO_2 into solution, isotopic signatures clearly demonstrate that, carbon in the meteoric water samples is sourced from the atmosphere. A positive correlation between DIC concentration and pH is observed for this group of samples, along with lower pCO_2 than expected for equilibrium with atmospheric CO_2. Meteoric-derived water samples evolve much closer to DIC concentration and $\delta^{13}C_{DIC}$ calculated for equilibrium with atmospheric CO_2 than the stream waters and the former group displays increasing DIC at invariant $\delta^{13}C_{DIC}$ (i.e., MWT and WO-TU in Fig. 4). Together with the decrease of pH observed for equilibration between drip water and tunnel atmosphere in the field, the above observations demonstrate that, the uptake of atmospheric CO_2 into alkaline solutions is an important mechanism in the formation of waters such as WO-TU. The evolution of the meteoric derived waters, which simultaneously increases pH, DIC and Mg concentration, can be rationalised by the incremental uptake of CO_2 and dissolution of brucite, resulting in further uptake of CO_2 at

increased pH. In this scenario, dissolution occurs under CO_2 limited conditions, allowing pH to increase, consistent with restricted CO_2 ingress into tailings at depth and slow uptake of CO_2 into solution observed during previous studies (Bea et al., 2011; Gras et al., 2015; Wilson et al., 2010; Wilson et al., 2014). A limitation in CO_2 supply during carbonation of mine tailings has been evoked in a number of previous studies as the rate limiting step for carbonation and increasing CO_2 supply is thought to bear considerable potential to accelerate the natural carbonation process in tailings storage facilities specifically designed for carbonation (Harrison et al., 2013; Power et al., 2013; Power et al., 2014; Wilson et al., 2010; Wilson et al., 2014). Our data, however, suggest that, waters close to saturation with respect to Mg-carbonates such as hydromagnesite can form despite limited CO_2 supply, because higher pH and therefore a proportional increase in carbonate ions can be attained in a closed system.

The uptake of CO_2 into solution cannot provide the driving force for carbonate precipitation, since it lowers pH and consequently carbonate saturation, as shown in Table SI 2 in the online version at http://dx.doi.org/10.1016/j.chemgeo.2016.04.014. Instead, the presented data confirm that, evaporation drives carbonate precipitation from meteoric-derived waters in the Woodsreef mine tailings. Previous studies have demonstrated that evaporation is not critical for carbonate precipitation in experimental mineral carbonation studies (Assima et al., 2012; Pronost et al., 2011). However, the availability of water and periodic wetting is critical in both experimental and natural settings (Assima et al., 2012) and represents a limiting factor for mineral carbonation under the semi-arid conditions prevailing at Woodsreef. Evaporation becomes important when the supply of water is limited, even in non-arid climates (Gras et al., 2015; Lechat et al., 2015; Lechat et al., 2016). At Woodsreef incipient and advanced evaporation of meteoric waters are reflected in the sampling context, the δ^2H and $\delta^{18}O$ signatures of WO-TU and WO-TOP, as well as in the high $\delta^{18}O$ signatures of carbonate precipitates relative to other Mg-carbonate precipitates worldwide (Kralik et al., 1989). Drip water sample WO-TU has to undergo at least 13 to 20% evaporation to reach the isotopic composition expected for equilibrium with the associated carbonate precipitate WO-TU_s (Table 4). However, even higher degrees of evaporation (>50%) are required to reach supersaturation with respect to hydromagnesite (Table 4). This agrees with previous studies of carbonate precipitation in ultramafic rocks, which identify evaporation as the main driving force for carbonate precipitation, with higher $\delta^{13}C$ and $\delta^{18}O$ in precipitates ascribed to evaporative enrichment of solutions before precipitation (Bea et al., 2011; Beinlich and Austrheim, 2012; Oskierski et al., 2013a; Power et al., 2009; Wilson et al., 2014).

Supplementary data to this article can be found online at http://dx.doi.org/10.1016/j.chemgeo.2016.04.014.

Acknowledgements

HCO acknowledges the University of Newcastle for a postgraduate research scholarship and the Australian Institute of Nuclear Science (AINSE) for a Postgraduate Research Award (AINSTU10108). We also acknowledge the constructive reviews by Prof G. Beaudoin and an anonymous reviewer, which have helped to significantly improve the manuscript. We would like to thank ANSTO staff for assistance in sample preparation and acquisition of radiocarbon data. We are indebted to Dr. E. Hobley for her contribution to the determination of $\delta^{13}C_{DIC}$ by IRMS and to Barbora Ghallager for the analysis of δ^2H and $\delta^{18}O$ of water samples. We acknowledge Dr. Suzanne Hollins, Dr. Judy Bailey and Professor Eric Kennedy for their support during this study.

References

Andersen, M.S., Meredith, K., Timms, W., Acworth, R.I., 2008. Investigation of δ18O and δ2H in the Namoi River catchment — elucidating recharge sources and the extent of surface water/groundwater interaction. Integrating Groundwater Science and Human Well-being Congress of IAH Toyama City, 36th, Japan, 26–31 October 2008.
Arvidson, R.S., MacKenzie, F.T., 1999. The dolomite problem: control of precipitation kinetics by temperature and saturation state. Am. J. Sci. 299, 257–288.
Ashley, P.M., 1997. Silica-carbonate alteration zones and gold mineralisation in the Great Serpentinite Belt, New England Orogen, New South Wales. In: PM, A., PG, F. (Eds.), Tectonics and Metallogenesis of the New England Orogen. Geol. Soc. Aust. Spec. Pub. 19, pp. 212–225.
Ashley, P.M., Brownlow, J.W., 1993. Silica-carbonate alteration zones in the Great Serpentinite Belt, southern New England Orogen: their nature and significance. In: Flood, P.G., Aitchison, J.C. (Eds.), New England Orogen. University of New England, Armidale, Australia, pp. 197–214.
Assayag, N., Rive, K., Ader, M., Jezequel, D., Agrinier, P., 2006. Improved method for isotopic and quantitative analysis of dissolved inorganic carbon in natural water samples. Rapid Commun. Mass Spectrom. 20, 2243–2251.
Assima, G.P., Larachi, F., Beaudoin, G., Molson, J., 2012. CO_2 sequestration in chrysotile mining residues — implications of watering and passivation under environmental conditions. Ind. Eng. Chem. Res. 51-26, 8726–8734.
Assima, G.P., Larachi, F., Beaudoin, G., Molson, J., 2013a. Dynamics of carbon dioxide uptake in chrysotile mining residues — effect of mineralogy and liquid saturation. Int. J. Greenhouse Gas Control 12, 124–135.
Assima, G.P., Larachi, F., Beaudoin, G., Molson, J., 2013b. Accurate and direct quantification of native brucite in serpentine ores — new methodology and implications for CO_2 sequestration by mining residues. Thermochim. Acta 566, 281–291.
Assima, G.P., Larachi, F., Molson, J., Beaudoin, G., 2014a. New tools for stimulating dissolution and carbonation of ultramafic mining residues. Can. J. Chem. Eng. 92-12, 2029–2038.
Assima, G.P., Larachi, F., Molson, J., Beaudoin, G., 2014b. Potential of Canadian mining residues for ambient carbonation. Carbon Capture J. 39, 7–10.
Australian Government Bureau of Meteorology, 2015. Climate data online: climate statistics for Australian locations, Barraba airport. http://www.bom.gov.au/climate/averages/tables/cw_054003.shtml (Accessed on 10/01/2015).
Bales, R.C., Morgan, J.J., 1985. Dissolution kinetics of chrysotile at pH 7 to 10. Geochim. Cosmochim. Acta 49 (11), 2281–2288.
Bar-Matthews, M., Ayalon, A., Matthews, A., Sass, E., Halicz, L., 1996. Carbon and oxygen isotope study of the active water-carbonate system in a karstic Mediterranean cave: implications for paleoclimate research in semiarid regions. Geochim. Cosmochim. Acta 60 (2), 337–347.
Bea, S.A., Wilson, S.A., Mayer, K.U., Dipple, G.M., Power, I.M., Gamazo, P., 2011. Reactive transport modelling of natural carbon sequestration in ultramafic mine tailings. Vadose Zone J. http://dx.doi.org/10.2136/vzj2011.0053.
Beinlich, A., Austrheim, H., 2012. In situ sequestration of atmospheric CO_2 at low temperature and surface cracking of serpentinized peridotite in mine shafts. Chem. Geol. 332-333, 32–44.
Brown R.E., Brownlow J.W., Krynen J.P. (1992) Manilla–Narrabri 1:250 000 Metallogenic Map SH/56–9, SH/55–12, Metallogenic Study and Mineral Deposit Data Sheets. NSW Geol. Surv., Metallogenic Map. Ser.
Bruni, J., Canepa, M., Chiodini, G., Cioni, R., Cipolli, F., Longinelli, A., Marini, L., Ottonello, G., Vetuschi, Z.M., 2002. Irreversible water-rock mass transfer accompanying the generation of the neutral, Mg–HCO3 and high pH, Ca–OH spring waters of the Genova province, Italy. Appl. Geochem. 17, 455–474.
Butman, D., Raymond, P.A., 2011. Significant efflux of carbon dioxide from streams and rivers in the United States. Nat. Geosci. 1294, 1–4.
Caillaud, J., Proust, D., Righi, D., 2006. Weathering sequences of rock-forming minerals in a serpentinite: influence of microsystems on clay mineralogy. Clay Clay Miner. 54-1, 87–100.
Cipolli, F., Gambardella, B., Marini, L., Ottonello, G., Zuccolini, M.V., 2004. Geochemistry of high pH waters from serpentinites of the Gruppo di Voltri (Genova, Italy) and reaction path modelling of CO_2 sequestration in serpentinite aquifers. Appl. Geochem. 19-5, 787–802.
Clark, I.D., Fritz, P., 1997. Environmental Isotopes in Hydrology. CRC Press (328 p).
Clark, I.D., Fontes, J.-C., Fritz, P., 1992. Stable isotope equilibria in travertine from high pH waters: laboratory investigations and field observations from Oman. Geochim. Cosmochim. Acta 56, 2042–2050.
Craig, H., 1961. Isotopic variations in meteoric waters. Science 133, 1702–1703.
Das Sharma, S., Patil, D.J., Gopalan, K., 2002. Temperature dependence of oxygen isotope fractionation of CO_2 from magnesite-phosphoric acid reaction. Geochim. Cosmochim. Acta 66, 589–593.
Davis, M., 2008. The CO_2 Sequestration Potential of the Ultramafic Rocks of the Great Serpentinite Belt, New South Wales Honours Thesis Department of Earth Sciences, University of Newcastle.
Dickson, A.G., Sabine, C.L., Christian, J.R., 2007. Guide to best practices for ocean CO_2 measurements. PICES Spec. Publ. 3 (http://www.cdiac.ornl.gov/oceans/Handbook_2007.html accessed on15/01/2016).
Doctor, D.H., Kendall, C., Sebesteyen, S.D., Shanley, J.B., Ohte, N., Boyer, E.W., 2008. Carbon isotope fractionation of dissolved inorganic carbon (DIC) due to outgassing of carbon dioxide from a headwater stream. Hydrol. Process. 22, 2410–2423.
Fairchild, I.J., Frisia, S., Borsato, A., Tooth, A.F., 2006. Speleothems in their geomorphic, hydrological and climatological context. In: Nash, D.J., McLaren, S.J. (Eds.), Geochemical Sediments and Landscapes. Blackwell Publishing Ltd, Oxford.
Fink, D., Hotchkis, M., Hua, Q., Jacobsen, G., Smith, A.M., Zoppi, U., Child, D., Mifsud, C., van der Gaast, H., Williams, A., Williams, M., 2004. The ANTARES AMS family at ANSTO. Nucl. Inst. Methods Phys. Res. B223-224, 109–115.
Friedli, H., Lotscher, H., Oeschger, H., Siegenthaler, U., Stauffer, B., 1986. Ice core record of the $^{13}C/^{12}C$ ratio of atmospheric CO_2 in the past two centuries. Nature 324 (6094), 237–238.

Gaillardet, J., Dupre, B., Louvat, P., Allegre, C.J., 1999. Global silicate weathering and CO_2 consumption rates deduced from the chemistry of large rivers. Chem. Geol. 159, 3–30.

Giammar, D.E., Bruant Jr., R.G., Peters, C.A., 2005. Forsterite dissolution and magnesite precipitation at conditions relevant for deep saline aquifer storage and sequestration of carbon dioxide. Chem. Geol. 217, 257–276.

Glen, R.A., 1971. The Geology of the Woodsreef Serpentinite, Near Barraba, New South Wales BSc (Hons) Thesis University of Sydney, Australia.

Glen, R.A., Butt, B.C., 1981. Chrysotile asbestos at Woodsreef, New South Wales. Econ. Geol. 76, 1153–1169.

Gonfiantini, R., 1986. Environmental isotopes in lake studies. In: Fritz, P., Fontes, J.-C. (Eds.), Handbook of Environmental Isotope Geochemistry. Elsevier, Amsterdam, pp. 113–168.

Gras, A., Beaudoin, G., Molson, J., Plante, B., Bussiere, B., Lemieux, J.M., Kandji, B., 2015. Carbon isotope evidence for passive mineral carbonation of mine wastes from the Dumont Nickel Project (Abitibi, Quebec). Fifth International Conference on Accelerated Carbonation for Environmental and Material Engineering. New York, 21–24 June 2015.

Gray, D.P., Harding, J.S., Elberling, B., Horton, T., Clough, T.J., Winterbourn, M.J., 2011. Carbon cycling in floodplain ecosystems: out-gassing and photosynthesis transmit soil $\delta^{13}C$ gradient through stream food webs. Ecosystems 14, 583–597.

Guo, B., Lackie, M.A., Flood, R.H., 2007. Upper crustal structure of the Tamworth Belt, New South Wales: constraints from new gravity data. Aust. J. Earth Sci. 54, 1073–1087.

Hänchen, M., Prigiobbe, V., Baciocchi, R., Mazzotti, M., 2008. Precipitation in the Mg-carbonate system — effects of temperature and CO_2 pressure. Chem. Eng. Sci. 63, 1012–1028.

Harrison, A.L., Power, I.M., Dipple, G.M., 2013. Accelerated carbonation of brucite in mine tailings for carbon sequestration. Environ. Sci. Technol. 47, 126–134.

Harrison, A.L., Dipple, G.M., Power, I.M., Mayer, K.U., 2015. Influence of surface passivation and water content on mineral reactions in unsaturated porous media: implications for brucite carbonation and CO_2 sequestration. Geochim. Cosmochim. Acta 148, 477–495.

Holland, H.D., Kirsiou, T.V., Huebner, J.S., Oxburgh, U.M., 1964. On some aspects of the chemical evolution of cave water. J. Geol. 72, 36–67.

Kakiuchi, M., Matsuo, S., 1979. Direct measurements of D/H and 18O/16O fractionation factors between vapor and liquid water in the temperature range from 10 to 40 °C. Geochem. J. 13, 307–311.

Kmetoni, J., 1984. Woodsreef mill tailings — investigation of potential for further utilization as a mineral resource (stage 1 — mineralogical composition). NSW Geol. Surv. Report GS1984/474.

Kralik, M., Aharon, P., Schroll, E., Zachmann, D., 1989. Carbon and oxygen isotope systematics of magnesites: a review. In: Möller, P. (Ed.), Magnesite. Monogr. Ser. Min. Depos. Vol. 28, pp. 197–223.

Lechat, K., Lemieux, J.M., Molson, J., Beaudoin, G., Hébert, R., 2015. Observations of CO_2 sequestration by mineral carbonation in milling wastes at Thetford Mines and evaluation of the potential for sequestration at the pilot scale (Quebec, Canada). Fifth International Conference on Accelerated Carbonation for Environmental and Material Engineering. New York, 21–24 June 2015.

Lechat, K., Lemieux, J.M., Molson, J., Beaudoin, G., Hébert, R., 2016. Field evidence of CO_2 sequestration by mineral carbonation in ultramafic milling wastes, Thetford Mines, Canada. Int. J. Greenhouse Gas Control 47, 110–121.

Marques, J.M., Carreira, P.M., Carvalho, M.R., Matias, M.J., Goff, F.E., Basto, M.J., Grace, R.C., Aires-Barros, L., Rocha, L., 2008. Origins of high pH mineral waters from ultramafic rocks, Central Portugal. Appl. Geochem. 23, 3278–3289.

McCutcheon, J., Dipple, G.M., Wilson, S.A., Southam, G., 2015. Production of magnesium-rich solutions by acid leaching of chrysotile: a precursor to field-scale deployment of microbially enabled carbonate mineral precipitation. Chem. Geol. 413, 119–131.

Mook, W.G., Bommerson, J.C., Staverman, W.H., 1974. Carbon isotope fractionation between dissolved bicarbonate and gaseous carbon dioxide. Earth Planet. Sci. Lett. 22, 169–176.

Munksgaard, N.C., Wurster, C.M., Bass, A., Bird, M.I., 2012. Extreme short-term stable isotope variability revealed by continuous rainwater analysis. Hydrol. Process. 26, 3630–3634.

O'Hanley, D.S., 1996. Serpentinites — Records of Tectonic and Petrological History. Oxford University Press, New York (277p).

O'Hanley, D.S., Offler, R., 1992. Characterisation of multiple serpentinisation, Woodsreef, New South Wales. Can. Mineral. 30, 1113–1126.

O'Neil, J.R., Barnes, I., 1971. C^{13} and O^{18} compositions in some fresh-water carbonates associated with ultramafic rocks and serpentinites: western United States. Geochim. Cosmochim. Acta 35, 687–697.

Oskierski, H.C., 2013. Natural Carbonation of Ultramafic Rocks in the Great Serpentinite Belt, New South Wales, Australia PhD Thesis The University of Newcastle, Australia.

Oskierski, H.C., Dlugogorski, B.Z., Jacobsen, G., 2013a. Sequestration of atmospheric CO_2 in chrysotile mine tailings of the Woodsreef Asbestos Mine, Australia: quantitative mineralogy, isotopic fingerprinting and carbonation rates. Chem. Geol. 358, 156–169.

Oskierski, H.C., Jacobsen, G., Dlugogorski, B.Z., 2013b. Sequestration of atmospheric CO_2 in a weathering-derived, serpentinite-hosted magnesite deposit: ^{14}C tracing of carbon sources and age constraints for a refined genetic model. Geochim. Cosmochim. Acta 122, 226–246.

Oskierski, H.C., Bailey, J.G., Kennedy, E.M., Jacobsen, G., Ashley, P.M., Dlugogorski, B.Z., 2013c. Formation of weathering-derived magnesite deposits in the New England Orogen, New South Wales, Australia: implications from mineralogy, geochemistry and genesis of the Attunga magnesite deposit. Mineral. Deposita 48-4, 525–542.

Park, A.-H.A., Fan, L.-S., 2004. CO_2 mineral sequestration: physically activated dissolution of serpentine and pH swing process. Chem. Eng. Sci. 59, 5241–5247.

Parkhurst, D.L., Appelo, C.A.J., 1999. User's guide to PHREEQC (version 2) — a computer program for speciation, batch reaction, one-dimensional transport, and inverse geochemical calculations. U.S. Geol. Surv. Water Res. Invest. Rep. 99–4259.

Paukert, A.P., Matter, J.M., Kelemen, P.B., Shock, E.L., Havig, J.R., 2012. Reaction path modelling of enhanced in situ CO_2 mineralisation for carbon sequestration in the peridotite of the Samail ophiolite, sultanate of Oman. Chem. Geol. 330-331, 86–100.

Pokrovsky, O.S., Schott, J., 2000. Kinetics and mechanisms of forsterite dissolution at 25 °C and pH from 1 t o12. Geochim. Cosmochim. Acta 64-19, 3313–3325.

Pokrovsky, O.S., Schott, J., 2004. Experimental study of brucite dissolution and precipitation in aqueous solutions: surface speciation and chemical affinity control. Geochim. Cosmochim. Acta 68-1, 31–45.

Pokrovsky, O.S., Golubev, S.V., Schott, H., 2005. Dissolution kinetics of calcite, dolomite and magnesite at 25 °C and 0 to 50 atm pCO_2. Chem. Geol. 217, 239–255.

Polsenaere, P., Abril, G., 2012. Modelling CO_2 degassing from small acidic rivers using water pCO_2, DIC and $\delta^{13}C$-DIC data (2012). Geochim. Cosmochim. Acta 91, 220–239.

Power, I.M., Wilson, S.A., Thom, J.M., Dipple, G.M., Gabites, J.E., Southam, G., 2009. The hydromagnesite playas of Atlin, British Columbia, Canada: a biogeochemical model for CO_2 sequestration. Chem. Geol. 260, 286–300.

Power, I.M., Harrison, A.L., Dipple, G.M., Wilson, S.A., Kelemen, P.B., Hitch, M., Southam, G., 2013. Carbon mineralization: from natural analogues to engineered system. Rev. Mineral. Geochem. 77, 305–360.

Power, I.M., McCutcheon, J., Harrison, A.L., Wilson, S.A., Dipple, G.M., Kelly, S., Southam, C., Southam, G., 2014. Strategizing carbon-neutral mines: a case for pilot projects. Minerals 4, 399–436.

Pronost, J., Beaudoin, G., Tremblay, J., Larachi, F., Duchesne, J., Hébert, R., Constantin, M., 2011. Carbon sequestration kinetic and storage capacity of ultramafic mining waste. Environ. Sci. Technol. 45–21, 9413–9420.

Pronost, J., Beaudoin, G., Lemieux, J.-M., Hebert, R., Constantin, M., Marcouiller, S., Klein, M., Duchesne, J., Molson, J.W., Larachi, F., Maldague, X., 2012. CO_2-depleted warm air venting from chrysotile milling waste (Thetford Mines, Canada): evidence for in-situ carbon capture from the atmosphere. Geology 40-3, 275–278.

Putnis, A., 2009. Mineral replacement reactions. Rev. Mineral. Geochem. 70, 87–124.

Raymond, P.A., Hartmann, J., Lauerwald, R., Sobek, S., McDonald, C., Hoover, M., Butman, D., Striegl, R., Mayorga, E., Humborg, C., Kortelainen, P., Duerr, H., Meybeck, M., Ciais, P., Guth, P., 2013. Global carbon dioxide emissions from inland waters. Nature 503, 355–359.

Ruddiman, W.F., 2013. Earth's Climate: Past and Future. third ed. W.H. Freeman (464 p).

Salata, G.G., Roelke, L.A., Cifuentes, L.A., 2000. A rapid and precise method for measuring stable carbon isotope ratios of dissolved inorganic carbon. Mar. Chem. 69, 153–161.

Saldi, G.D., Jordan, G., Schott, J., Oelkers, E.H., 2009. Magnesite growth rates as a function of temperature and saturation state. Geochim. Cosmochim. Acta 73, 5646–5657.

Svanosio, R.A., 2000. Exploration license number 5490 "Woodsreef". Annual Technical Report GS2000/358.

Toyer, G.S., Main, S., 1978. Some environmental investigations at the Woodsreef asbestos mine. NSW Geol. Surv. Rep. GS 1978/382.

Van Geldern, R., Schulte, P., Mader, M., Baier, A., Barth, J.A.C., 2015. Spatial and temporal variations of pCO_2, dissolved inorganic carbon and stable isotopes along a temperate karstic watercourse. Hydrol. Process. 29, 3423–3440.

Vickery N.M., Brown R.E., Percival I.G. (2010) Manilla 1:100000 Geological Sheet 9036 Explanatory Notes. NSW Geol. Surv., Maitland, Australia.

Wilson, S.A., Raudsepp, M., Dipple, G.M., 2006. Veryfying and quantifying carbon fixation in minerals from serpentine-rich mine tailings using the Rietveld method with X-ray powder diffraction data. Am. Mineral. 91, 1331–1341.

Wilson, S.A., Dipple, G.M., Power, I.M., Thom, J.M., Anderson, R.G., Raudsepp, M., Gabites, J.E., Southam, G., 2009. Carbon dioxide fixation within mine wastes of ultramafic-hosted ore deposits: examples from the Clinton Creek and , Canada. Econ. Geol. 104, 95–112.

Wilson, S.A., Barker, S.L., Dipple, G.M., Atudorei, V., 2010. Isotopic disequilibrium during uptake of atmospheric CO_2 into mine process waters: implications for CO_2 sequestration. Environ. Sci. Technol. 44, 9522–9529.

Wilson, S.A., Dipple, G.M., Power, I.M., Barker, S.L.L., Fallon, S.J., Southam, G., 2011. Subarctic weathering of mineral wastes provides a sink for atmospheric CO_2. Environ. Sci. Technol. 45, 7727–7736.

Wilson, S.A., Harrison, A.L., Dipple, G.M., Power, I.M., Barker, S.L.L., Mayer, K.U., Fallon, S.J., Raudsepp, M., Southam, G., 2014. Offsetting of CO_2 emissions by air capture in mine tailings at the Mount Keith nickel mine, Western Australia: rates, controls and prospects for carbon neutral mining. Int. J. Greenhouse Gas Control 25, 121–140.

Zappa, C.J., McGillis, W.R., Raymond, P.A., Edson, J.B., Hintsa, E.J., Zemmelink, H.J., Dacey, J.W.H., Ho, D.T., 2007. Environmental turbulent mixing control on air water gas exchange in marine and aquatic systems. Geophys. Res. Lett. 34, L10601.

Zeebe, R.E., 2012. History of seawater carbonate chemistry, atmospheric CO_2 and ocean acidification. Annu. Rev. Earth Planet. Sci. 40, 141–150.